PCCP

Accepted Manuscript

ROYAL SOCIETY OF CHEMISTRY

www.rsc.org/pccp

Tracing the Origins of Transient Overshoots for Binary Mixture Diffusion in Microporous Crystalline Materials

Rajamani Krishna

Van 't Hoff Institute for Molecular Sciences, University of Amsterdam, Science Park 904,

1098 XH Amsterdam, The Netherlands

Footnotes

Van 't Hoff Institute for Molecular Sciences, University of Amsterdam, Science Park 904, 1098 XH Amsterdam, The Netherlands. Fax: 31 20 525 5604; Tel: 31 20 627 0990; E-mail: r.krishna@contact.uva.nl

† Electronic Supplementary Information (ESI) available: Electronic supplementary information (ESI) available: See DOI: 10.1039/c1csXXXXX. Supporting Information Available. This document provides details of (a) pure component isotherm fits, (b) modelling of mixture adsorption equilibrium, (c) calculation of thermodynamic correction factors, (d) Maxwell-Stefan diffusion equations for describing transient uptake of mixtures, and (e) methodology for simulation of transient uptake, membrane permeation, and transient breakthroughs in fixed beds. Also included as ESI are video animations of transient development of loadings within particles, and across membranes. These animations provide some "feel" of spatio-temporal overshoots in loadings during transient uptake and membrane permeation. See DOI: 10.1039/b000000x/

ABSTRACT

Separations of mixtures using microporous crystalline materials are normally achieved by exploiting differences in the adsorption strengths of the constituent species. The focus of the current investigation is on diffusion-selective separations that exploit differences in intra-crystalline diffusivities of guest molecules. A number of experimental investigations report overshoots in intra-crystalline loadings of the more mobile species during transient mixture uptake. Analogous overshoots in fluxes occur for mixture permeation across thin microporous membrane layers. The attainment of supra-equilibrium loadings is a common characteristic of diffusion-selective separations; this allows the over-riding of adsorption selectivities. The primary objective of the current investigation is to demonstrate that the Maxwell-Stefan diffusion formulation, using chemical potential gradients as driving forces, is capable of providing a quantitative description of the temporal and spatial overshoots found in the diverse experimental works. The origins of the overshoots can be traced to thermodynamic coupling effects that emanate from sizable off-diagonal contributions of the matrix of thermodynamic correction factors. If thermodynamic coupling effects are neglected, the overshoots are not realized. It is also demonstrated that while the transport of the more mobile partner is uphill of its loading gradient, its transport is downhill the gradient of its chemical potential. The deliberate exploitation of uphill diffusion to achieve difficult separations is highlighted.

1. Introduction

Microporous adsorbents such as zeolites, carbon molecular sieves, metal-organic frameworks (MOFs), and zeolitic imidazolate framework (ZIFs) have potential in a variety of applications such as CO_2 capture, natural gas purification, and O_2/N_2 separations.[1-3] Such separations are commonly conducted in fixed bed adsorbers.[4] The fixed bed devices are operated in a cyclical manner with adsorption and desorption cycles; the operations are intrinsically transient in nature, i.e. the concentrations in the bulk fluid phase, and within the particles, vary both with distance along the adsorber, z, and time, t.[4-7] Most commonly, the separation performance in a fixed-bed adsorber is dictated by mixture adsorption equilibrium. Intra-particle diffusion limitations cause distended breakthrough characteristics and usually lead to diminished separation effectiveness.[2, 7] However, there are some instances in which diffusional effects over-ride the influence of mixture adsorption equilibrium and is the prime driver for separations.[3, 4, 8, 9]

For the separation of O_2/N_2 mixtures using LTA-4A, LTA-5A, or NaX, the adsorption selectivity is in favor of N_2 due to the larger permanent quadrupole moment of N_2 compared to that of O_2.[9, 10] This implies that an adsorption based process would selectively adsorb N_2, and pure O_2 can be produced in the adsorption cycle.[11, 12] For production of purified N_2, it is desirable to selectively adsorb O_2. Selectivity towards O_2 can be achieved by choosing LTA-4A zeolite or carbon molecular sieve (CMS).[9-13] Due to its smaller cross-sectional dimension, 3.1 Å for O_2, compared to 3.3 Å for N_2, the intra-particle diffusivity of O_2 is significantly higher than that of N_2 in both LTA-4A and CMS.[9, 11-13] The significantly lower diffusivity of N_2 has the consequence that purified N_2 breaks through earlier in a fixed bed adsorber and can be recovered in purified form during the initial stages of transient breakthroughs.[2, 4, 9]

Another example is the separation of N_2/CH_4 mixtures that is important in the context of natural gas upgrading because the presence of N_2 reduces the heating value. Some natural gas reserves contain up

to 20% N_2; reduction to less than about 2% is required in order to meet the pipeline specifications for natural gas. For most known adsorbents, the adsorption selectivity favors CH_4 that has a higher polarizability.[9, 10] A practical approach is to rely on diffusion selectivities by using microporous adsorbents such as LTA-4A zeolite and Ba-ETS-4.[14-16] The cross-sectional dimension of CH_4 is 3.7 Å, which is higher than that of N_2 (3.3 Å); consequently, the diffusivity of N_2 is significantly higher in LTA-4A and Ba-ETS-4. Purified natural gas can be recovered during the early stages of transient breakthroughs in fixed-bed adsorbers packed with LTA-4A and Ba-ETS-4.[2, 7]

A common characteristic of diffusion selective separations is that the transient mixture uptake within a porous particle exhibits overshoots in the loading of the more mobile component. The experimental data of Chen et al.[13] for transient uptake of O_2/N_2 mixture within a CMS particle shows an overshoot for the more mobile O_2; see Figure 1a. For transient uptake of N_2/CH_4 mixtures, overshoots in the loading of the more mobile N_2 have been reported for LTA-4A zeolite;[14] see Figure 1b. The experimental data of Titze et al.[17] for transient uptake of *n*-hexane(nC6)/2-methylpentane(2MP) mixtures in MFI zeolite crystal, exposed to an equimolar binary gas mixture at constant total pressure (= 2.6 Pa) shows a pronounced overshoot in the uptake of the more mobile linear isomer nC6; supra-equilibrium loadings of nC6 are attained during transient approach to equilibrium; see Figure 1c.

The experimental data of Saint-Remi et al.[18] for transient uptake of ethanol/1-propanol mixtures within SAPO-34 crystals, that is the structural analog of CHA zeolite, are shown in Figure 1d. The more mobile ethanol exhibits a pronounced overshoot in the uptake transience, exceeding the final equilibrated loading.

In more recent experimental investigations using interference microscopy (IFM), Binder et al.[19] and Lauerer et al.[20] have monitored the uptake of CO_2, and C_2H_6 within crystals of DDR zeolite exposed to a bulk gas phase consisting of 1:1, 2:1, and 3:1 CO_2/C_2H_6 mixtures. In all three sets of experiments, supra-equilibrium CO_2 loadings are attained during transient equilibration. A significant aspect of the Binder, and Lauerer experiments, is that both the spatial loadings (along the radial direction of crystal; see Figures 2a, and 2b) and spatial-averaged uptakes (see Figures 3a, 3b, and 3c) of guest molecules

have been monitored. Their experiments show overshoots, both spatial and temporal, in the loadings of the more mobile CO_2. The radial profile for 2:1 CO_2/C_2H_6 mixtures, for example, (Figure 2a) shows that the CO_2 peaks migrate to the crystal interiors as time progresses; the magnitude of the peaks reduce in magnitude until equilibration.

In all the above mentioned sets of uptake experiments, with diverse guest/host combinations, the attainment of supra-equilibrium loadings signals uphill diffusion.[21]

Diffusion-selective separations can also be achieved in membrane constructs, by allowing the feed mixture to permeate through thin microporous films. Such membrane devices are normally operated under steady-state conditions. Experimental data on transient permeation of CH_4/nC_4H_{10},[22] H_2/nC_4H_{10},[23] nC_4H_{10}/iso-C_4H_{10},[24] nC6/2MP,[25] nC6/2,3-dimethylbutane (23DMB),[25] benzene/p-xylene,[26] m-xylene/p-xylene,[27] and o-xylene/m-xylene/p-xylene[27] mixtures across MFI membranes show overshoots in the flux of the more mobile partners during the transient approach towards steady-state.

The primary objective of this article is to demonstrate that the spatial and temporal overshoots in the afore-mentioned sets of uptake and membrane experiments can be modelled quantitatively using the Maxwell-Stefan (M-S) diffusion formulation.[7, 21] The secondary objective is to show that while the more mobile species experiences transport uphill of the gradient of its molar loading, it is downhill the gradient of its chemical potential.

The Electronic Supporting Information (ESI) accompanying this publication provides details of fitting of pure component isotherms, modelling of mixture adsorption equilibrium, calculations of chemical potential gradients, solution of the partial differential equations describing intra-crystalline diffusion, and details of simulations of transient uptake, membrane permeation, and fixed-bed breakthroughs.

2. The Maxwell-Stefan formulation for micropore diffusion

The key to modelling overshoots in transient mixture diffusion lies in the proper choice of driving forces for diffusion of constituent species. Within microporous materials, the guest molecules exist in the adsorbed phase, and the Gibbs adsorption equation[28] in differential form is

$$A d\pi = \sum q_i d\mu_i \tag{1}$$

The quantity A on the left side of Equation (1) is the surface area per kg of framework, with units of m^2 per kg of the framework of the crystalline material; q_i is the molar loading of component i in the adsorbed phase with units moles per kg of framework; μ_i is the molar chemical potential of component i. The spreading pressure, π, has the same units as surface tension, i.e. N m^{-1}; indeed, the spreading pressure is the negative of the surface tension.[29]

For describing the unary transport of bound moisture in wood, Babbitt[30, 31] suggested the use of the gradient of the spreading pressure $\partial\pi/\partial r$ as thermodynamically correct driving force. Essentially, he postulated that the force exerted per mole of adsorbate, $-(A/q_i)(\partial\pi/\partial r)$, is balanced by friction, or drag, between the mobile adsorbates and the material surface

$$-\frac{A}{q_i}\frac{\partial\pi}{\partial r} = \frac{RT}{Đ_i}u_i \tag{2}$$

where u_i is the velocity of motion of the adsorbate with respect to the framework material. The unary diffusivity $Đ_i$, with the units m^2 s^{-1}, is interpreted as an inverse drag coefficient between the adsorbate and the surface. If we define N_i as the number of moles of species i transported per m^2 of crystalline material per second

$$N_i \equiv \rho q_i u_i \tag{3}$$

where ρ is the framework density with units of kg m^{-3}, we obtain the flux relation

$$-\rho\frac{A}{RT}\frac{\partial\pi}{\partial r} = \frac{N_i}{Đ_i} \tag{4}$$

In view of Equation (1), the Babbitt equation (4) is equivalent to the Maxwell-Stefan (M-S) formulation,[7, 21, 32] commonly written for unary diffusion in the form

$$-\rho\frac{q_i}{RT}\frac{\partial\mu_i}{\partial r} = \frac{N_i}{Đ_i} \tag{5}$$

The use of chemical potential gradients as proper driving forces has also been emphasized in the classic text of Ruthven.[28]

In extending Equation (5) to describe binary mixture diffusion in micropores, we need to include interactions between the guest species. The M-S equations[32-35] are usually written in the following form

$$-\rho\frac{q_1}{RT}\frac{\partial\mu_1}{\partial r}=\frac{x_2N_1-x_1N_2}{Đ_{12}}+\frac{N_1}{Đ_1};$$
$$-\rho\frac{q_2}{RT}\frac{\partial\mu_2}{\partial r}=\frac{x_1N_2-x_2N_1}{Đ_{12}}+\frac{N_2}{Đ_2} \qquad (6)$$

The diffusivities $Đ_1$ and $Đ_2$ retain the same physical significance as for unary diffusion; these are inverse drag coefficients of the respective species experienced with the material surface. Indeed, a persuasive advantage of the M-S formulation over the Onsager formulation is that the $Đ_i$ often retain the same magnitude and loading dependence characteristics as the corresponding unary micropore diffusivities.[32, 33, 36] The $Đ_{12}$ is the exchange coefficient representing interaction between component 1 with component 2. At the molecular level, the $Đ_{12}$ reflects how the facility for transport of species 1 correlates with that of species 2. For mesoporous materials with pores in the 20 Å to 100 Å size range the values of the exchange coefficient $Đ_{12}$ are the nearly the same as the binary *fluid phase* M-S diffusivity, $Đ_{12,\mathrm{fl}}$, over the entire range of pore concentrations. [32, 33, 37, 38] Procedures for estimation of the $Đ_{12,\mathrm{fl}}$ are available in Poling et al.,[39] and therefore this provides a convenient starting point for the estimation of the $Đ_{12}$. For microporous materials, the exchange coefficients $Đ_{12}$ are lower than the corresponding values of $Đ_{12,\mathrm{fl}}$ by a factor that depends on the pore size, connectivity and topology.[32, 33, 37, 38] Alternative Maxwell-Stefan formulations for mixture diffusion in microporous maerials are available in the literature;[5, 40-42] these use occupancies $\theta_i = q_i / q_{i,sat}$ instead of the adsorbed phase mole fractions, x_i; for further details see the ESI.

For microporous crystals in equilibrium with an ideal gas mixture, $\frac{\partial \mu_i}{\partial r} = RT \frac{\partial \ln p_i}{\partial r} = RT \frac{1}{p_i} \frac{\partial p_i}{\partial r}$. The gradients in the chemical potential can be related to the gradients of the molar loadings, q_i, by defining thermodynamic correction factors Γ_{ij}

$$\frac{q_i}{RT} \frac{\partial \mu_i}{\partial r} = \sum_{j=1}^{2} \Gamma_{ij} \frac{\partial q_j}{\partial r}; \quad \Gamma_{ij} = \frac{q_i}{p_i} \frac{\partial p_i}{\partial q_j}; \quad i, j = 1,2 \tag{7}$$

The thermodynamic correction factors Γ_{ij} can be calculated by differentiation of the model describing mixture adsorption equilibrium. Generally speaking, the Ideal Adsorbed Solution Theory (IAST) of Myers and Prausnitz[29] is the preferred method for estimation of mixture adsorption equilibrium, especially for cases in which the saturation capacities of the constituents are largely different.[43, 44] The IAST may however fail in case of segregated adsorption and occurrence of molecular clustering. In special cases, the mixed-gas Langmuir model

$$\frac{q_i}{q_{i,sat}} = \theta_i = \frac{b_i p_i}{1 + b_1 p_1 + b_2 p_2}; \quad i = 1,2 \tag{8}$$

may be of adequate accuracy. If Equation (8) is used to describe mixture adsorption equilibrium, the elements Γ_{ij} can be calculated explicitly from

$$\Gamma_{ij} = \delta_{ij} + \left(\frac{q_{i,sat}}{q_{j,sat}} \right) \frac{\theta_i}{1 - \theta_1 - \theta_2}; \quad i = 1,2 \tag{9}$$

Combining Equations (6), and (7) we obtain[32-34]

$$\begin{pmatrix} N_1 \\ N_2 \end{pmatrix} = -\frac{\rho}{1 + \frac{x_1 Đ_2}{Đ_{12}} + \frac{x_2 Đ_1}{Đ_{12}}} \begin{bmatrix} Đ_1 \left(1 + \frac{x_1 Đ_2}{Đ_{12}} \right) & \frac{x_1 Đ_1 Đ_2}{Đ_{12}} \\ \frac{x_2 Đ_1 Đ_2}{Đ_{12}} & Đ_2 \left(1 + \frac{x_2 Đ_1}{Đ_{12}} \right) \end{bmatrix} \begin{bmatrix} \Gamma_{11} & \Gamma_{12} \\ \Gamma_{21} & \Gamma_{22} \end{bmatrix} \begin{pmatrix} \frac{\partial q_1}{\partial r} \\ \frac{\partial q_2}{\partial r} \end{pmatrix} \tag{10}$$

The ratios $Đ_1/Đ_{12}$, and $Đ_2/Đ_{12}$ quantify the degrees of correlations.[32, 34] As illustration, Figure 4 shows Molecular Dynamics (MD) data on $Đ_1/Đ_{12}$ for equimolar binary $H_2(1)/CH_4(2)$ mixtures in a

variety of host materials. The data are compared as function of the total pore concentration, $c_t = (q_1 + q_2)/V_p$ where V_p is the accessible pore volume.[37] For any guest/host combination, $Đ_1/Đ_{12}$ is seen to increase as the pore concentration increases; this implies that correlation effects are expected to be stronger at higher pressures. We consider correlation effects to be strong when $Đ_1/Đ_{12} > 1$; $Đ_2/Đ_{12} > 1$; this scenario holds for mixture diffusion in mesoporous materials, one-dimensional (1D) channel structures (e.g. MgMOF-74), intersecting channels (e.g. MFI, BEA zeolite), and "open" structures (e.g. NaX zeolite, CuBTC, IRMOF-1) consisting of large cages separated by wide windows. Strong correlation effects cause slowing-down of more-mobile-less-strongly-adsorbed molecules by tardier-more-strongly-adsorbed-partner species.[32, 34]

Conversely, when $Đ_1/Đ_{12} << 1$; $Đ_2/Đ_{12} << 1$, correlation effects are of negligible importance. This scenario holds for materials such as LTA, ZIF-8, CHA, DDR, and ERI that consist of cages separated by windows in the 3.4 Å – 4.2 Å size range.[32-34, 45] Molecules jump one-at-a-time across the narrow windows, and the assumption of negligible correlations is justified; in this scenario, Equation (10) simplifies to yield[7, 21]

$$N_1 = -\rho Đ_1 \frac{\partial(\Gamma_{11}q_1 + \Gamma_{12}q_2)}{\partial r}; \quad N_2 = -\rho Đ_2 \frac{\partial(\Gamma_{21}q_1 + \Gamma_{22}q_2)}{\partial r} \tag{11}$$

The quantities $\Gamma_{11}q_1 + \Gamma_{12}q_2$, and $\Gamma_{21}q_1 + \Gamma_{22}q_2$ have the units mol kg^{-1} and may be regarded as the "thermodynamically corrected" measures of component loadings of components 1 and 2. The intra-crystalline fluxes N_1, and N_2 are, respectively, proportional to the gradients of these corrected loadings. Round et al.[46] were the first to use Equation (11) to model transient uptake in zeolites and provide an provide a theoretical basis for transient overshoots. Equation (11) has also been used by Brandani et al.[47] to interpret co- and counter-diffusion of benzene and xylenes in MFI zeolite.

Depending on the specific guest/host combination that is under consideration, either equation (10) or (11) is used to describe the fluxes for binary mixture diffusion. The theoretical framework is valid for any type of microporous material, such as zeolites, MOFs, ZIFs or activated carbon. For ordered

crystalline materials, molecular simulations may be used as guidelines for determining the diffusivities and adsorption equilibrium.[7]

3. Transient CO_2/C_2H_6 mixture uptake in DDR crystals

We begin with modeling of CO_2/C_2H_6 mixture uptake in DDR zeolite crystals with the objective of simulating the Binder, and Lauerer experiments.[19, 20] DDR is a cage-type zeolite with 278 Å^3 sized cages separated by narrow windows with dimensions 3.65 Å × 4.37 Å; see Figures S12, S13, and S14 of the ESI. Molecular Dynamics (MD) simulations[34, 45, 48, 49] have established that CO_2 molecules jump lengthwise across the windows. The cross-section dimension of a CO_2 molecule is 3.03 Å, significantly lower than that of C_2H_6 that has a cross-section of 3.76 Å; see Figure S15. Using MD simulations[1, 34, 45, 48] as guidelines, we anticipate the diffusivity of CO_2 to be about 1-3 orders of magnitude higher than that of C_2H_6. Inter-cage hopping of guest molecules in DDR occur one-at-a-time across windows; i.e. the molecular jumps are not correlated,[34, 45, 48] and equation (11) is the appropriate flux expression to use.

The accuracy of the use of the mixed-gas Langmuir model (8) to describe CO_2/C_2H_6 mixture adsorption equilibrium in DDR is established by comparison with calculations using the Ideal Adsorbed Solution Theory (IAST);[29] see Figure S17. The agreement between the mixed-gas Langmuir and IAST model is good because of the limited range of loadings considered. Consequently, Equation (9) is used to determine the elements Γ_{ij}. Figure 5 presents calculations of Γ_{ij}, expressed as a function of total mixture loading, q_t, for 3:1 ratio of partial pressures of CO_2(1) and C_2H_6(2) in the gas phase. The off-diagonal elements Γ_{12}, and Γ_{21} become increasingly important with increased mixture loadings, q_t. In particular, it is noteworthy that the ratio Γ_{12}/Γ_{11} gets progressively closer to unity as the mixture loading, q_t, increases. This implies that thermodynamic coupling effects are of particular significance for the uptake of CO_2 from CO_2/C_2H_6 gas mixtures.

For transient mixture uptake under conditions of finite loadings, Equations (7), and (9) imply that the chemical potential gradient of species *i* is influenced by the gradients in the loading of both species in

the mixture; this influence is termed thermodynamic coupling. Thermodynamic coupling is always of importance for mixture uptake in microporous materials under conditions of finite loadings.

For most crystal geometries, model representation as an equivalent sphere is an acceptable approximation for modelling transient uptake.[28] The hexagonal-shaped crystals of DDR zeolite, used in the Binder, and Lauerer[19, 20] experiments are modelled as spherical crystals of radius r_c. The radial distribution of molar loadings, q_i, is obtained from a solution of a set of differential equations describing the uptake[7, 28]

$$\frac{\partial q_i(r,t)}{\partial t} = -\frac{1}{\rho}\frac{1}{r^2}\frac{\partial}{\partial r}\left(r^2 N_i\right) \tag{12}$$

The fluxes N_i, in turn, are related to the radial gradients in the molar loadings by equation (11). At time t = 0, i.e. the initial conditions, the molar loadings $q_i(r,0)$ at all locations r within the crystal are uniform (zero loadings). For all times $t \geq 0$, the exterior of the crystal is brought into contact with a bulk gas mixture at partial pressures $p_i(r_c,t)$ that is maintained constant till the crystal reaches thermodynamic equilibrium with the surrounding gas mixture.

$$t \geq 0; \quad q_i(r_c,t) \text{ in equilibrium with the initial values } p_i(r_c,t) \tag{13}$$

At any time t, during the transient approach to thermodynamic equilibrium, the spatial-averaged component loadings within the crystallites of radius r_c are calculated by integrating over the volume of the crystal

$$\bar{q}_i(t) = \frac{3}{r_c^3}\int_0^{r_c} q_i(r,t) r^2 dr \tag{14}$$

The experimental $\bar{q}_i(t)$ data of Binder, and Lauerer[19, 20] with 1:1, 2:1, and 3:1 CO_2/C_2H_6 gas mixtures are indicated by the symbols in Figure 3, panels a, b, and c. For each data set, the parameters $Đ_1/r_c^2$, and $Đ_2/r_c^2$ were chosen to get a good match with the experiments; the simulation results with use of equation (11) are shown by the continuous solid lines in Figure 3. The fitted values of $Đ_1/r_c^2$, and

$Đ_2/r_c^2$, appear to correlate with the corresponding loadings, q_1, and q_2, in the adsorbed mixture at final equilibration; see Figure 6. The overshoots in the spatial-averaged CO_2 loadings in all three experimental campaigns are captured adequately by the M-S model equations (11), in conjunction with the fitted diffusivity values.

In the Henry regime of adsorption, where the fractional occupancies are vanishingly small, we have the special case that elements of the matrix of thermodynamic factors Γ_{ij} equals the Kronecker delta

$$\theta_i \to 0; \quad \Gamma_{ij} \to \delta_{ij}; \quad \frac{q_i}{RT}\frac{\partial \mu_i}{\partial r} \to \frac{\partial q_i}{\partial r}; \quad i,j = 1,2 \tag{15}$$

In this scenario of negligible thermodynamic coupling, equation (11) reduces to yield the uncoupled flux relations

$$N_i = -\rho Đ_i \frac{\partial q_i}{\partial r}; \quad i = 1,2; \quad \text{neglecting thermodynamic coupling} \tag{16}$$

The simulation results neglecting thermodynamic coupling effects are indicated by the dashed lines in Figures 3, panels a, b, and c. In this scenario, the overshoots in the spatial-averaged CO_2 loadings disappear. The inescapable conclusion to be drawn is that thermodynamic coupling effects are the root cause of the transient overshoots of the more mobile species in binary mixture uptake in DDR crystals.

Figures 7a, and 7b present the simulation results for the transient development of component loadings along the radius of DDR crystal (center, $r = 0$; surface of crystal, $r = r_c$) monitored at different times for uptake from 2:1 CO_2/C_2H_6 gas mixtures; analogous data for 1:1, and 3:1 CO_2/C_2H_6 gas mixtures are provided in Figures S25, and S27. Video animations of transient development of spatial loadings have been uploaded as ESI; these animations provide some feel of the spatio-temporal overshoots experienced by CO_2 during transient uptake.

The CO_2 peak migrates from the surface regions to the crystal interiors as time progresses, in qualitative agreement with the corresponding experimental profiles in Figure 2a. Despite the fact that the values of $Đ_1/r_c^2$, and $Đ_2/r_c^2$ are fitted to match the spatial-averaged $\bar{q}_i(t)$, we should not expect a one-to-one correspondence in the data on the $q_1(r,t)$, and $q_2(r,t)$; this is because of the use of a spherical

geometry to model the hexagonal DDR crystals employed in the experiments. Due to the presence of surface barriers, the experimentally determined surface loadings change with time. However, in our simulations instantaneous equilibration at the surface is assumed; consequently, there are quantitative differences in the radial profiles obtained in the two sets. The spatial overshoot of CO_2 loadings is a clear indication of uphill transport. In order to determine its origins, we need to examine the mixture adsorption thermodynamics in further detail. From the data on the $q_1(r,t)$, and $q_2(r,t)$ we determined the quantities $\Gamma_{11}q_1(r,t)+\Gamma_{12}q_2(r,t)$, and $\Gamma_{21}q_1(r,t)+\Gamma_{22}q_2(r,t)$ that are thermodynamically corrected measures of component loadings of components 1 and 2. Figures 7c, and 7d show the transient development of corrected loadings along the radius of DDR crystal. In terms of corrected loadings, there is no spatial overshoot of CO_2; this implies that CO_2 is not transported uphill of the gradient of its chemical potential.

It now remains to demonstrate that the use of corrected loadings serves to rationalize the experimentally observed spatio-temporal overshoots in the CO_2 loadings in the Binder, and Lauerer experiments.[19, 20] From the experimental data on the $q_1(r,t)$, and $q_2(r,t)$ in Figure 2, we determined the quantities $\Gamma_{11}q_1(r,t)+\Gamma_{12}q_2(r,t)$, and $\Gamma_{21}q_1(r,t)+\Gamma_{22}q_2(r,t)$ that are thermodynamically corrected measures of component loadings of components 1 and 2; the results are presented in Figures 8a, and 8b. In terms of corrected loadings, there are no spatio-temporal overshoots for CO_2. Indeed, the equilibration of both CO_2, and C_2H_6 proceeds in the same, conventional, manner. Both simulations (Figure 7), and experiments (Figure 8) confirm that the transport of CO_2 is downhill of the chemical potential gradient.

Though not mentioned in the papers by Binder, and Lauerer,[19, 20] the results in Figures 3 suggests that CO_2 removal from C_2H_6-rich streams can be achieved in fixed beds packed with DDR particles; in this case the separations rely both on differences in intra-crystalline diffusivities and thermodynamic coupling effects. Figure 9 shows the simulations of transient breakthrough of 10/90 CO_2/C_2H_6 mixtures through fixed bed adsorber packed with DDR crystals operating at 298 K, and total pressure p_t = 100 kPa. We note that C_2H_6 breaks through earlier and can be recovered in purified form during the early

stages of the transient operations. The separation relies on the significantly higher intra-crystalline diffusivity of CO_2. If there is no intra-crystalline diffusional limitation, CO_2 breaks through earlier and the purification strategy will be ineffectual.

4. Transient mixture uptake in other guest/host combinations

Precisely analogous conclusions can be drawn by comparison of M-S model simulations with the experimental data for O_2/N_2 uptake in CMS,[13] N_2/CH_4 uptake in LTA-4A,[14] and n-hexane (nC6)/2-methylpentane (2MP) uptake in MFI zeolite;[17] see Figure 1, panels a, b, and c. The experimentally observed overshoots in the three experimental sets are adequately captured by the M-S equation (11) that includes thermodynamic coupling; these are indicated by the continuous solid lines in Figure 1. Video animations of the transient development of loadings along the crystal radius show spatio-temporal overshoots of the more mobile N_2, O_2, and nC6 in the three respective experiments. If thermodynamic coupling effects are neglected, the more mobile species displays a monotonous approach to equilibrium, as indicated by the dashed lines in Figure 1.

Overshoots in the transient uptake of the more mobile partner species have also been reported for benzene/p-xylene in ZSM-5,[50, 51] benzene/ethylbenzene in ZSM-5,[50, 51] n-heptane/benzene in NaX,[52] ethane/n-butane, ethane/n-pentane, and n-butane/n-pentane mixtures in extrudates of activated carbon (AC);[53] these data are amenable to interpretation in the same manner as in the foregoing examples.[7, 21] Simulation results for these systems confirm that the experimental observed overshoots are ascribable to thermodynamic coupling influences; see Figures S46-S50.

Transient overshoots of the mobile species may also occur for adsorption-diffusion-reaction within MFI catalysts; see Figures S86 – S94.

5. Influence of the ratio of M-S diffusivities, $Đ_1/Đ_2$, on overshoots

From a practical standpoint, it is of interest to know under what set of conditions transient overshoots may be expected to occur. To get some insights into this question, we investigated binary $C_3H_6(1)/C_3H_8(2)$ mixture uptake in ZIF-8. In ZIF-8, the adsorption strength of the saturated propane is

slightly higher than that of propene; at 303 K, the ratio of Langmuir constants, b_2/b_1 = 1.07. The windows of ZIF-8 have a dimension of about 3.3 Å. Due to subtle differences in bond lengths and bond angles of propene, and propane (see Figure 10), the diffusivity of C_3H_6 is higher than that of C_3H_8.[54] In the experimental study of Li et al.,[55] a value of the ratio $Đ_1/Đ_2$ =125 has been obtained based on the data on pure component uptakes. The membrane permeation experiments of Pan et al.[56] and Liu et al.[57] indicate permeation selectivities in the range 30 – 35, that are consistent with the choice $Đ_1/Đ_2 \approx 40$. We undertook a parametric study of the influence of the ratio of $Đ_1/Đ_2$; three values for the ratio were chosen: 2, 10, and 125. In these three scenarios the diffusivity of the saturated alkane was held constant at the value $Đ_2/r_c^2 = 1.2\times10^{-4}$ s^{-1}. The simulation results are shown in Figure 10. The overshoot in the uptake of the unsaturated propene persists for the ratios $Đ_1/Đ_2$ = 10 and $Đ_1/Đ_2$ = 125; see video animations of the transient development of loadings. However, for the choice $Đ_1/Đ_2$ = 2, the overshoot in the C_3H_6 uptake is practically non-existent. We conclude that for sizable overshoots to occur, the diffusivity of the more mobile species must be significantly higher than that of the tardier partner species. Interestingly, C_3H_6 exhibits undershoot phenomena during desorption; see Figure S55.

6. Separating mono- and di-branched alkanes by exploiting uphill diffusion in MFI zeolite

The isomerization of alkanes, for the purposes of octane improvement, is a process of importance in the petroleum industry.[2, 7, 58] The product from the isomerization reactor consists of an equilibrium distribution of linear alkanes, mono-branched alkanes, and di-branched alkanes with carbon numbers in the 5-7 range. The values of the Research Octane Number (RON) increases with the degree of branching; for hexane isomers: the RON values are: nC6 (n-hexane) = 30, 2MP (2-methylpentane) = 74.5, 3MP (3-methylpentane) = 75.5, 22DMB (2,2-dimethylbutane) = 94, 23DMB (2,3-dimethylbutane) = 105. Therefore, the di-branched isomers 22DMB and 23DMB are preferred products for incorporation into the high-octane gasoline pool. The separation of di-branched 22DMB and 23DMB from linear nC6 can be achieved by molecular sieving using, say, LTA-5A zeolite. The separation of di-branched

isomers from mono-branched isomers is much more challenging. An important strategy that is effective for this separation is the exploitation of configurational entropy effects,[7, 44, 59] combined with uphill diffusion of the more mobile guest species in MFI zeolite. As illustration, consider the separation of a ternary gaseous 2-methylbutane (2MB)/2MP/22DMB mixture. The adsorption and diffusivity data for MFI extrudates are reported by Jolimaître et al.[60, 61] The adsorption hierarchy that is dictated by configurational entropy considerations[7, 44, 59] is 2MP > 22DMB > 2MB. The diffusivity hierarchy is also dictated by subtle differences in molecular configurations: $Đ_{2MB}/r_c^2 = 7.5\times10^{-3}$ s^{-1} > $Đ_{2MP}/r_c^2 = 5\times10^{-3}$ s^{-1} >> $Đ_{22DMB}/r_c^2 = 6.25\times10^{-5}$ s^{-1}.

Transient uptake inside MFI extrudates exposed to a ternary 2MB/2MP/22DMB gas phase mixture shows overshoots for the two mono-branched isomers 2MB, and 2MP; see Figure 11a. If thermodynamic coupling effects are ignored, the component loadings of all three components exhibit monotonous approaches to equilibrium. Both mono-branched alkanes 2MB, and 2MP experience uphill diffusion that allows the attainment of supra-equilibrium loadings. As a consequence of uphill diffusion, the transient breakthrough experimental data (indicated by symbols in Figure 11b) show the elution sequence 22DMB, 2MB, followed by 2MP. This sequence is the desirable one, because the high-octane di-branched 22DMB can be recovered from the gas mixture exiting the adsorber for incorporation into the gasoline pool, during the initial transience.

The experimental breakthrough data are in good agreement with breakthrough simulations that take take proper account of thermodynamic coupling, using the flux relations Equation (11); see continuous solid lines in Figure 11b. If thermodynamic coupling effects are ignored (i.e. no uphill diffusion), the separation is less effective and is indicated by the dashed lines in Figure 11b.

7. Separating linear alcohols by exploiting uphill diffusion in CHA zeolite

The quantitative modelling of the transient uptake of ethanol/1-propanol mixtures in SAPO-34, shown in Figure 1d, is not possible because the required unary isotherm data are not available. For this reason, we carried out uptake simulations in CHA zeolite that has the same topology as SAPO-34; the unary

isotherms for adsorption of 1-alcohols in CHA, determined from Configurational-Bias Monte Carlo (CBMC) simulations have been reported in the literature.[7, 44, 62] Transient uptake simulation results taking the mobility of ethanol to be 10 times that of 1-propanol are presented in Figure 12a. The continuous solid lines are transient uptake simulations use Equation (11); in this scenario, substantial overshoots of ethanol are found. The dashed lines are the calculations using uncoupled flux equation (16); in this scenario, no ethanol overshoot is detected.

The uphill transport of ethanol can be exploited for ethanol/1-propanol separations in fixed beds carried out under pore saturation conditions. At pore saturation conditions, the ethanol/1-propanol mixture adsorption equilibrium favors the shorter alcohol because of the higher packing efficiency of the shorter alcohol within the cages of CHA.[7, 44, 62] Uphill transport of ethanol enhances the efficacy of this separation, and the component that elutes first in fixed-bed adsorbers is the longer chain alcohol; see Figure 12b. The breakthrough experimental data of Remy et al.[63] for separation of ethanol/1-propanol mixtures in a fixed bed adsorber provides confirmation of the simulated elution sequence.

8. Overshoots in mixture permeation across microporous membrane layers

Geus et al.[22] report experimental data on transient 50/50 CH_4/nC_4H_{10} mixture permeation across an MFI membrane; the flux of the more mobile CH_4 exhibits a pronounced overshoot during the approach to steady state. Simulations were undertaken to rationalize the Geus experiments. Molecular Dynamics (MD) simulation data,[33, 34] indicate that correlation effects for CH_4/nC_4H_{10} mixture diffusion within the intersecting channels of MFI are particularly strong; using the MD data as guidelines we choose $Đ_1/Đ_2$ = 10; and $Đ_1/Đ_{12} = 2$ for quantitative modelling. The mixture adsorption equilibrium is determined using the IAST. The transient permeation fluxes N_i, defined in terms of the cross-sectional area of the membrane, need to take account of both correlations and thermodynamic coupling; Equation (10) is the appropriate flux expression to use. The N_i are determined by solving the set of partial differential equations

$$\frac{\partial q_i(z,t)}{\partial t} = -\frac{1}{\rho}\frac{\partial}{\partial z}\left(N_i\right) \tag{17}$$

where z is the distance coordinate along the direction of membrane thickness.

The boundary conditions are the partial pressures and component molar loadings at the upstream (z = 0) and downstream ($z = \delta$) faces of the membrane

$$\begin{aligned} z &= 0; \quad p_i = p_{i0}; \quad q_i = q_{i0} \\ z &= \delta; \quad p_i = p_{i\delta}; \quad q_i = q_{i\delta} \end{aligned} \tag{18}$$

The continuous solid lines in Figure 13 are the numerical simulations to Equation (17), in conjunction with the fluxes determined using Equation (10), Equation (11), or Equation (**16**). The plot shows the normalized fluxes $N_1/\left(\rho q_{10} Đ_1/\delta\right)$, and $N_2/\left(\rho q_{20} Đ_2/\delta\right)$ as steady-state is approached. The inclusion of of correlations in the flux calculations serves to reduce the magnitude of the overshoot in CH_4; this is because of the slowing-down of the more mobile within the intersecting channels of MFI zeolite. We conclude that correlation effects cannot cause overshoots; indeed, their inclusion only serves to smear them out. If both correlations, and thermodynamic coupling effects are neglected, the overshoot in CH_4 disappears altogether; thermodynamic coupling is the sole cause of transient permeation overshoots.

Figure 14a shows the transient development of CH_4 loadings, q_1, along the MFI membrane thickness, monitored at different times from start of the permeation. The CH_4 loadings display spatio-temporal overshoots during the transient approach to steady-state, indicative of uphill transport; this is clearly evidenced in the video animations included as ESI. In terms of corrected loadings, $\Gamma_{11}q_1 + \Gamma_{12}q_2$, the loading profiles of CH_4 displays monotonous characteristics; see Figure 14b. These results prove that CH_4 permeation is downhill of the chemical potential gradient.

The experimental data of Bakker[23] for transient permeation H_2/nC_4H_{10} mixture across an MFI membrane shows a maximum in the flux of the more mobile H_2; the rationalization these experiments proceeds along identical lines as in the foregoing analysis; the detailed simulation results are summarized in Figures S72 –S74.

For permeation of nC6/2MP mixtures across an MFI membrane, Matsufuji et al.[25] report experimental data showing overshoots in the nC6 flux during transient approach to steady-state. The overshoot in the nC6 flux is precisely analogous to the nC6 loading overshoot observed in the Titze experiments (see Figure 1c). Indeed, the nC6 flux overshoot manifests in membrane permeation simulations using the same diffusivity data used to model the Titze mixture uptake; see Figures S75–S78.

The experimental data of Matsufuji et al.[27] for transient permeation of (a) 50/50 m-xylene/p-xylene, and (b) 24/50/25 p-xylene/m-xylene/o-xylene mixtures across MFI membrane show a maximum in the flux of p-xylene which is the most mobile of the three xylene isomers; see Figure S79. The origin of the flux overshoot of p-xylene can be traced to thermodynamic coupling effects; see Figure S80.

For nC_4H_{10}/iso-C_4H_{10} mixture permeation across a MFI membrane, curious overshoots and undershoots, in the transient retentate and permeate concentrations have been reported in the experiments of Courthial et al.[24] As evidenced in the simulation results in Figure S81, the origins of the nC4 overshoots can be traced to the influence of thermodynamic coupling.

Pervaporation of water/alcohol mixtures is an important process in the processing industry, and a wide variety of membrane materials has been used, including polymers, zeolites (e.g. CHA, LTA, MFI, FAU, DDR), ZIF-8, and mixed matrix membranes.[64-68] Due to the high mobility of water molecules, uphill transport of water is evidenced in simulations of transient water/ethanol permeation across DDR and LTA-4A membranes (see Figures S82 –S85), but there is no experimental confirmation of the overshoot phenomena observed in these simulations.

9. Conclusions

The Maxwell-Stefan diffusion equations with chemical potential gradients as driving forces are able to quantitatively reproduce the temporal and spatial overshoots in the loading of the more mobile guest molecules for transient uptake in different guest/host combinations: CO_2/C_2H_6/DDR, N_2/CH_4/LTA-4A, O_2/N_2/CMS, nC6/2MP/MFI, and ethanol/1-propanol/CHA. The origins of the overshoots in the loadings of the more mobile guests can be traced to thermodynamic coupling effects that emanate from sizable off-diagonal contributions of the matrix of thermodynamic correction factors, $[\Gamma]$. During transient

approach to equilibrium, supra-equilibrium loadings within the particles are observed, signaling the phenomenon of uphill transport. The use of the corrected loadings $\Gamma_{11}q_1(r,t)+\Gamma_{12}q_2(r,t)$, and $\Gamma_{21}q_1(r,t)+\Gamma_{22}q_2(r,t)$ results in monotonous equilibration, without overshoots; see Figure 7, and Figure 8. While the transport of the more mobile species is uphill of the gradient in molar loading, the transport is downhill the gradient of chemical potential. If thermodynamic coupling effects are neglected, no overshoots are realized.

Our analysis also suggests the possibility of exploitation of uphill transport to achieve difficult separations. For example, the results in Figure 9 suggests that CO_2 can be selectively adsorbed from C_2H_6 in fixed beds.

Analogous conclusions hold for transient CH_4/nC_4H_{10}, H_2/nC_4H_{10}, nC6/2MP, and nC_4H_{10}/iso-C_4H_{10} mixture permeation across MFI membranes. In these three cases, overshoots disappear when thermodynamic coupling and correlation effects are both neglected. Transient overshoots in membrane permeation can be exploited to recover more mobile species during the early stages of the transient approach to steady-state.

The discussions and results presented in this article are of importance in the proper modelling of diffusion-selective separations carried in fixed-bed adsorbers, catalytic reactors, and membrane permeation devices.

10. Notation

A	surface area per kg of framework, $m^2\ kg^{-1}$
b_i	Langmuir adsorption constant for species i, Pa^{-1}
c_i	molar concentration, $mol\ m^{-3}$
$Đ_i$	M-S diffusivity for molecule-wall interaction, $m^2\ s^{-1}$
$Đ_{12}$	M-S exchange coefficient, $m^2\ s^{-1}$
f_i	partial fugacity of species i, Pa
k_1	forward reaction rate constant, s^{-1}
k_2	backward reaction rate constant, s^{-1}
L	length of packed bed adsorber, m
N_i	molar flux of species i with respect to framework, $mol\ m^{-2}\ s^{-1}$
p_i	partial pressure of species i in mixture, Pa
p_t	total system pressure, Pa
q_i	component molar loading of species i, $mol\ kg^{-1}$
$q_{i,sat}$	molar loading of species i at saturation, $mol\ kg^{-1}$
q_t	total molar loading in mixture, $mol\ kg^{-1}$
$\bar{q}_i(t)$	spatial-averaged component uptake of species i, $mol\ kg^{-1}$
r	radial direction coordinate, m
r_c	radius of crystallite, m
R	gas constant, 8.314 $J\ mol^{-1}\ K^{-1}$
t	time, s
u_i	velocity of motion of adsorbate species i with respect to the framework material, $m\ s^{-1}$
v	interstitial gas velocity in packed bed, $m\ s^{-1}$
V_p	pore volume, $m^3\ kg^{-1}$
T	absolute temperature, K
z	distance coordinate, m

Greek letters

δ	thickness of microporous membrane, m
δ_{ij}	Kronecker delta, dimensionless
ε	voidage of packed bed, dimensionless
Γ_{ij}	thermodynamic factors, dimensionless
$[\Gamma]$	matrix of thermodynamic factors, dimensionless
μ_i	molar chemical potential of component *i*, J mol^{-1}
μ_i^0	molar chemical potential of component *i* at standard state, J mol^{-1}
π	spreading pressure, N m^{-1}
θ_i	fractional occupancy of component *i*, dimensionless
ρ	framework density, kg m^{-3}
τ	time, dimensionless

Subscripts

i	referring to component *i*
t	referring to total mixture

11. References

1. R. Krishna and J. M. van Baten, *Phys. Chem. Chem. Phys.*, 2011, **13**, 10593-10616.
2. R. Krishna, *RSC Adv.*, 2015, **5**, 52269-52295.
3. J. Kärger, D. M. Ruthven and D. N. Theodorou, *Diffusion in Nanoporous Materials*, Wiley - VCH, Weinheim, 2012.
4. D. M. Ruthven, S. Farooq and K. S. Knaebel, *Pressure swing adsorption*, VCH Publishers, New York, 1994.
5. R. Krishna and R. Baur, *Sep. Purif. Technol.*, 2003, **33**, 213-254.
6. Y. He, R. Krishna and B. Chen, *Energy Environ. Sci.*, 2012, **5**, 9107-9120.
7. R. Krishna, *Microporous Mesoporous Mater.*, 2014, **185**, 30-50.
8. R. T. Yang, *Gas separation by adsorption processes*, Butterworth, Boston, 1987.
9. R. T. Yang, *Adsorbents: Fundamentals and Applications*, John Wiley & Sons, Inc., Hoboken, New Jersey, 2003.
10. S. Sircar and A. L. Myers, in *Handbook of Zeolite Science and Technology*, eds. S. M. Auerbach, K. A. Carrado and P. K. Dutta, Marcel Dekker, New York, 2003, pp. 1063-1104.
11. S. Farooq, M. N. Rathor and K. Hidajat, *Chem. Eng. Sci.*, 1993, **48**, 4129-4141.
12. S. Farooq, *Gas Sep. Purif.*, 1995, **9**, 205-212.
13. Y. D. Chen, R. T. Yang and P. Uawithya, *A.I.Ch.E.J.*, 1994, **40**, 577-585.
14. H. W. Habgood, *Canad. J. Chem.*, 1958, **36**, 1384-1397.
15. S. J. Bhadra and S. Farooq, *Ind. Eng. Chem. Res.*, 2011, **50**, 14030-14045.
16. B. Majumdar, S. J. Bhadra, R. P. Marathe and S. Farooq, *Ind. Eng. Chem. Res.*, 2011, **50**, 3021-3034.
17. T. Titze, C. Chmelik, J. Kärger, J. M. van Baten and R. Krishna, *J. Phys. Chem. C*, 2014, **118**, 2660-2665.
18. J. C. Saint-Remi, G. V. Baron and J. F. M. Denayer, *J. Phys. Chem. C*, 2013, **117**, 9758-9765.
19. T. Binder, A. Lauerer, C. Chmelik, J. Haase, J. Kärger and D. M. Ruthven, *Ind. Eng. Chem. Res.*, 2015, **54**, 8997-9004.
20. A. Lauerer, T. Binder, C. Chmelik, E. Miersemann, J. Haase, D. M. Ruthven and J. Kärger, *Nat. Commun.*, 2015, **6**, 7697. http://dx.doi.org/doi:10.1038/ncomms8697
21. R. Krishna, *Chem. Soc. Rev.*, 2015, **44**, 2812-2836.
22. E. R. Geus, H. van Bekkum, W. J. W. Bakker and J. A. Moulijn, *Microporous Mater.*, 1993, **1**, 131-147.
23. W. J. W. Bakker, Ph.D. Thesis, Ph.D. Dissertation, Delft University of Technology, 1999.
24. L. Courthial, A. Bandot, M. Tayakout-Fayolle and C. Jallut, *A.I.Ch.E.J.*, 2013, **59**, 959-970.
25. T. Matsufuji, K. Watanabe, N. Nishiyama, Y. Egashira, M. Matsukata and K. Ueyama, *Ind. Eng. Chem. Res.*, 2000, **39**, 2434-2438.
26. R. Kolvenbach, N. Al-Yassir, S. S. S.S. Al-Khattaf, O. C. Gobin, J. H. Ahn, A. Jentys and J. A. Lercher, *Catal. Today*, 2011, **168**, 147-157.
27. T. Matsufuji, N. Nishiyama, M. Matsukata and K. Ueyama, *J. Membr. Sci.*, 2000, **178**, 25-34.
28. D. M. Ruthven, *Principles of Adsorption and Adsorption Processes*, John Wiley, New York, 1984.
29. A. L. Myers and J. M. Prausnitz, *A.I.Ch.E.J.*, 1965, **11**, 121-130.
30. J. D. Babbitt, *Canad. J. Res.*, 1950, **28 A**, 449-474.
31. J. D. Babbitt, *Canad. J. Phys.*, 1951, **29**, 427-436.
32. R. Krishna, *Chem. Soc. Rev.*, 2012, **41**, 3099-3118.
33. R. Krishna, *J. Phys. Chem. C*, 2009, **113**, 19756-19781.

34. R. Krishna and J. M. van Baten, *J. Membr. Sci.*, 2013, **430**, 113-128.
35. R. Krishna and J. M. van Baten, *J. Phys. Chem. C*, 2010, **114**, 11557-11563.
36. R. Krishna and J. M. van Baten, *Chem. Eng. Sci.*, 2008, **63**, 3120-3140.
37. R. Krishna and J. M. van Baten, *Chem. Eng. Sci.*, 2009, **64**, 3159-3178.
38. R. Krishna and J. M. van Baten, *J. Membr. Sci.*, 2011, **383**, 289-300.
39. B. E. Poling, J. M. Prausnitz and J. P. O'Connell, *The Properties of Gases and Liquids*, 5th Edition edn., McGraw-Hill, New York, 2001.
40. F. Kapteijn, J. A. Moulijn and R. Krishna, *Chem. Eng. Sci.*, 2000, **55**, 2923-2930.
41. A. I. Skoulidas, D. S. Sholl and R. Krishna, *Langmuir*, 2003, **19**, 7977-7988.
42. R. Krishna and J. M. van Baten, *Microporous Mesoporous Mater.*, 2008, **109**, 91-108.
43. R. Krishna and J. R. Long, *J. Phys. Chem. C*, 2011, **115**, 12941-12950.
44. R. Krishna, *Phys. Chem. Chem. Phys.*, 2015, **17**, 39-59.
45. R. Krishna and J. M. van Baten, *Microporous Mesoporous Mater.*, 2011, **137**, 83-91.
46. G. F. Round, H. W. Habgood and R. Newton, *Sep. Sci.*, 1966, **1**, 219-244.
47. S. Brandani, M. Jama and D. M. Ruthven, *Ind. Eng. Chem. Res.*, 2000, **39**, 821-828.
48. R. Krishna and J. M. van Baten, *Sep. Purif. Technol.*, 2008, **61**, 414-423.
49. R. Krishna and J. M. van Baten, *J. Membr. Sci.*, 2010, **360**, 323-333.
50. W. Niessen and H. G. Karge, *Microporous Mater.*, 1993, **1**, 1-8.
51. H. G. Karge, *C.R. Chim.*, 2005, **8**, 303-319.
52. J. Kärger and M. Bülow, *Chem. Eng. Sci.*, 1975, **30**, 893-896.
53. X. Hu and D. D. Do, *Chem. Eng. Sci.*, 1992, **47**, 1715-1725.
54. R. Krishna and J. M. van Baten, *J. Phys. Chem. C*, 2012, **116**, 23556-23568.
55. K. Li, D. H. Olson, J. Seidel, T. J. Emge, H. Gong, H. Zeng and J. Li, *J. Am. Chem. Soc.*, 2009, **131**, 10368-10369.
56. Y. Pan, T. Li, G. Lestari and Z. Lai, *J. Membr. Sci.*, 2012, **390-391**, 93-98.
57. D. Liu, X. Ma, H. Xi and Y. S. Lin, *J. Membr. Sci.*, 2014, **451**, 85-93.
58. Z. R. Herm, B. M. Wiers, J. M. Van Baten, M. R. Hudson, P. Zajdel, C. M. Brown, N. Maschiocchi, R. Krishna and J. R. Long, *Science*, 2013, **340**, 960-964.
59. T. J. H. Vlugt, R. Krishna and B. Smit, *J. Phys. Chem. B*, 1999, **103**, 1102-1118.
60. E. Jolimaître, M. Tayakout-Fayolle, C. Jallut and K. Ragil, *Ind. Eng. Chem. Res.*, 2001, **40**, 914-926.
61. E. Jolimaître, K. Ragil, M. Tayakout-Fayolle and C. Jallut, *A.I.Ch.E.J.*, 2002, **48**, 1927-1937.
62. R. Krishna and J. M. van Baten, *Sep. Purif. Technol.*, 2011, **76**, 325-330.
63. T. Remy, J. C. Saint-Remi, R. Singh, P. A. Webley, G. V. Baron and J. F. M. Denayer, *J. Phys. Chem. C*, 2011, **115**, 8117-8125.
64. P. Peng, B. Shi and Y. Lan, *Separ. Sci. Technol.*, 2011, **46**, 234-246.
65. K. Sato, K. Aoki, K. Sugimoto, K. Izumi, S. Inoue, J. Saito, S. Ikeda and T. Nakane, *Microporous Mesoporous Mater.*, 2008, **115**, 184-188.
66. K. Sato, K. Sugimoto, N. Shimosuma, T. Kikuchi, T. Kyotani and T. Kurata, *J. Membr. Sci.*, 2012, **409-410**, 82-95.
67. J. Kuhn, J. M. Castillo-Sanchez, J. Gascon, S. Calero, D. Dubbeldam, T. J. H. Vlugt, F. Kapteijn and J. Gross, *J. Phys. Chem. C*, 2009, **113**, 14290-14301.
68. M. Pera-Titus, C. Fité, V. Sebastián, E. Lorente, J. Llorens and F. Cunill, *Ind. Eng. Chem. Res.*, 2008, **47**, 3213-3224.

12. Caption for Figures

Figure 1. (a) Experimental data of Chen et al.[13] for spatial-averaged transient uptake of $O_2(1)/N_2(2)$ mixture in carbon molecular sieve (CMS) at 300 K exposed to binary gas mixtures at partial pressures p_1 =109.6 kPa; p_2 = 432.56 kPa. (b) Experimental data of Habgood[14] on transient uptake of $N_2(1)/CH_4(2)$ mixture within LTA-4A crystals, exposed to binary gas mixtures at 194 K and partial pressures p_1 =50.9 kPa; p_2 = 49.1 kPa. (c) Experimental data (Run 1) of Titze et al.[17] for transient uptake of nC6/2MP mixtures in MFI zeolite. (d) Experimental data of Saint-Remi et al.[18] for transient uptake of ethanol/1-propanol mixtures within SAPO-34. The continuous solid lines are based on the flux equation (**11**). The dashed lines are the calculations using uncoupled flux equation (**16**). Further simulation details are provided in the ESI.

Figure 2. (a, b) Experimental data of Binder, and Lauerer[19, 20] for transient development of molar loadings of (a) $CO_2(1)$, and (b) $C_2H_6(2)$ along the radius of DDR crystal monitored at different times from start of the uptake. In the bulk gas phase 298 K, p_1 = 40 kPa, p_2 = 20 kPa.

Figure 3. (a, b, c) Experimental data of Binder, and Lauerer[19, 20] (indicated by symbols) for spatial-averaged transient uptake of (a) 1:1 (b) 2:1, and (c) 3:1 $CO_2(1)/C_2H_6(2)$ gas mixtures within crystals of DDR zeolite. The continuous solid lines are based on the flux equation (**11**).The dashed lines are the calculations using uncoupled flux equation (**16**). Further simulation details are provided in the ESI.

Figure 4. MD simulation data for the degree of correlations, $Đ_1/Đ_{12}$, for diffusion of equimolar binary $H_2(1)/CH_4(2)$ mixtures at 300 K in a variety of host materials, as a function of the total pore concentration, $c_t = (q_1 + q_2)/V_p$.

Figure 5. Elements of the matrix of thermodynamic correction factors Γ_{ij} as a function of total mixture loading, q_t, calculated using the mixed-gas Langmuir model for binary $CO_2(1)/C_2H_6(2)$ mixture adsorption in DDR for 3:1 ratio of partial pressures in the gas phase. In these calculations the total gas pressure, p_t, was varied from 1 to 100 kPa.

Figure 6. The dependence of the diffusivities $Đ_1/r_c^2$, and $Đ_2/r_c^2$ for $CO_2(1)$, and $C_2H_6(2)$ in DDR on the corresponding component loadings, q_1, and q_2, in the adsorbed phase at equilibrium.

Figure 7. Simulation results for transient development of (a, b) molar loadings, and (c, d) "corrected" molar loadings of $CO_2(1)$, and $C_2H_6(2)$ along the radius of DDR crystal (center, $r = 0$; surface of crystal, $r = r_c$) monitored at different times from start of the uptake. In the bulk gas phase 298 K, $p_1 = 40$ kPa, $p_2 = 20$ kPa.

Figure 8. Experimental data of Binder, and Lauerer[19, 20] for transient development of "corrected" molar loadings of (a) $CO_2(1)$, and (b) $C_2H_6(2)$ along the radius of DDR crystal monitored at different times from start of the uptake. In the bulk gas phase 298 K, $p_1 = 40$ kPa, $p_2 = 20$ kPa.

Figure 9. Transient breakthrough of 10/90 CO_2/C_2H_6 mixtures through fixed bed adsorber packed with DDR crystals operating at 298 K, and total pressure p_t = 100 kPa. The parameter values are: L = 0.3 m; voidage of bed, ε = 0.4; interstitial gas velocity, v = 0.1 m/s; radius of crystallite, r_c = 40 μm; $Đ_1/r_c^2$ = 0.00125 s^{-1}; $Đ_1/Đ_2$ = 1333. The y-axis is the gas phase concentration at the adsorber outlet, normalized with respect to the feed concentrations at the inlet. The x-axis is the dimensionless time, $\tau = tv/L$, obtained by dividing the actual time, t, by the characteristic time, L/v. Further simulation details are provided in the ESI.

Figure 10. Simulations of transient uptake of C_3H_6(1)/C_3H_8(2) within crystals of ZIF-8 at 303 K. In the simulations $Đ_2/r_c^2$ = 1.2×10^{-4} s^{-1}. The ratios $Đ_1/Đ_2$ have three different values: 2, 10, and 125. The three sets of simulations are based on the flux equation (**11**). Further simulation details are provided in the ESI.

Figure 11. (a) Transient uptake inside MFI crystal exposed to a gas phase 2MB/2MP/22DMB mixture at 473 K. (b) Comparison of transient breakthrough experimental data of Jolimaître et al.[61] with transient breakthrough simulations. The partial pressures of the components in the bulk gas phase at the inlet are p_1 = 81 kPa; p_2 = 177 kPa; p_2 = 106 kPa. These conditions correspond to Run 20 of Jolimaître et al.[61] Diffusional effects are quantified with $Đ_{2MB}/r_c^2$ = 0.0075 s^{-1} $Đ_{2MP}/r_c^2$ = 0.005 s^{-1}; $Đ_{2MP}/Đ_{22DMB}$ = 80. The continuous solid lines represent uptake simulations include thermodynamic coupling using the flux relations Equation (11). The dashed lines represent uptake simulations ignoring thermodynamic coupling and use uncoupled flux equation (16). See video animations of the transient uptake within crystal and transient breakthrough in bed.

Figure 12. (a) Simulations of transient uptake of ethanol(1)/1-propanol(2) mixtures within CHA crystals, exposed to binary gas mixtures with partial fugacities $f_{\text{ethanol}} = f_{\text{1-propanol}} = 0.5$ MPa. (b) Breakthrough simulations for ethanol/1-propanol mixtures in a fixed bed adsorber packed with CHA. The Maxwell-Stefan diffusivities: $Đ_{ethanol}/r_c^2 = 4\times10^{-3}$ s^{-1}; $Đ_{1-propanol}/r_c^2 = 4\times10^{-5}$ s^{-1}. The continuous solid lines are the calculations with flux relations Equation (11). The dashed lines are the calculations neglecting thermodynamic coupling and using uncoupled flux equation (16).

Figure 13. Simulations of transient 50/50 CH_4(1)/nC_4H_{10}(2) membrane permeation. The diffusivity data used are: $\rho Đ_1/\delta = 7.18\times10^{-3}$ kg m^{-2} s^{-1}, $\rho Đ_2/\delta = 7.18\times10^{-4}$ kg m^{-2} s^{-1}; $Đ_1/Đ_2 = 10$; $Đ_1/Đ_{12} = 2$; membrane thickness $\delta = 200$ μm; partial pressures in upstream membrane compartment, $p_{10} = p_{20} = 50$ kPa. The downstream compartment is placed under vacuum, i.e. $p_{1\delta} = p_{2\delta} \approx 0$. The loadings at the upstream face are: $q_{10} = 0.0063$ mol kg^{-1}, $q_{20} = 1.638$ mol kg^{-1}. Three different flux expressions are used in the calculations: Equation (10), Equation (11), and Equation (**16**).

Figure 14. Simulations of transient 50/50 CH_4(1)/nC_4H_{10}(2) MFI membrane permeation: transient development of (a) CH_4 loadings, q_1, and (b) corrected loadings, $\Gamma_{11}q_1 + \Gamma_{12}q_2$, along the MFI membrane thickness (upstream face, $z = 0$; downstream face, $z = \delta$) monitored at different times from start of the permeation. In these simulations, correlation effects and thermodynamic coupling effects are accounted for by use of Equation (10).

MS Fig 1

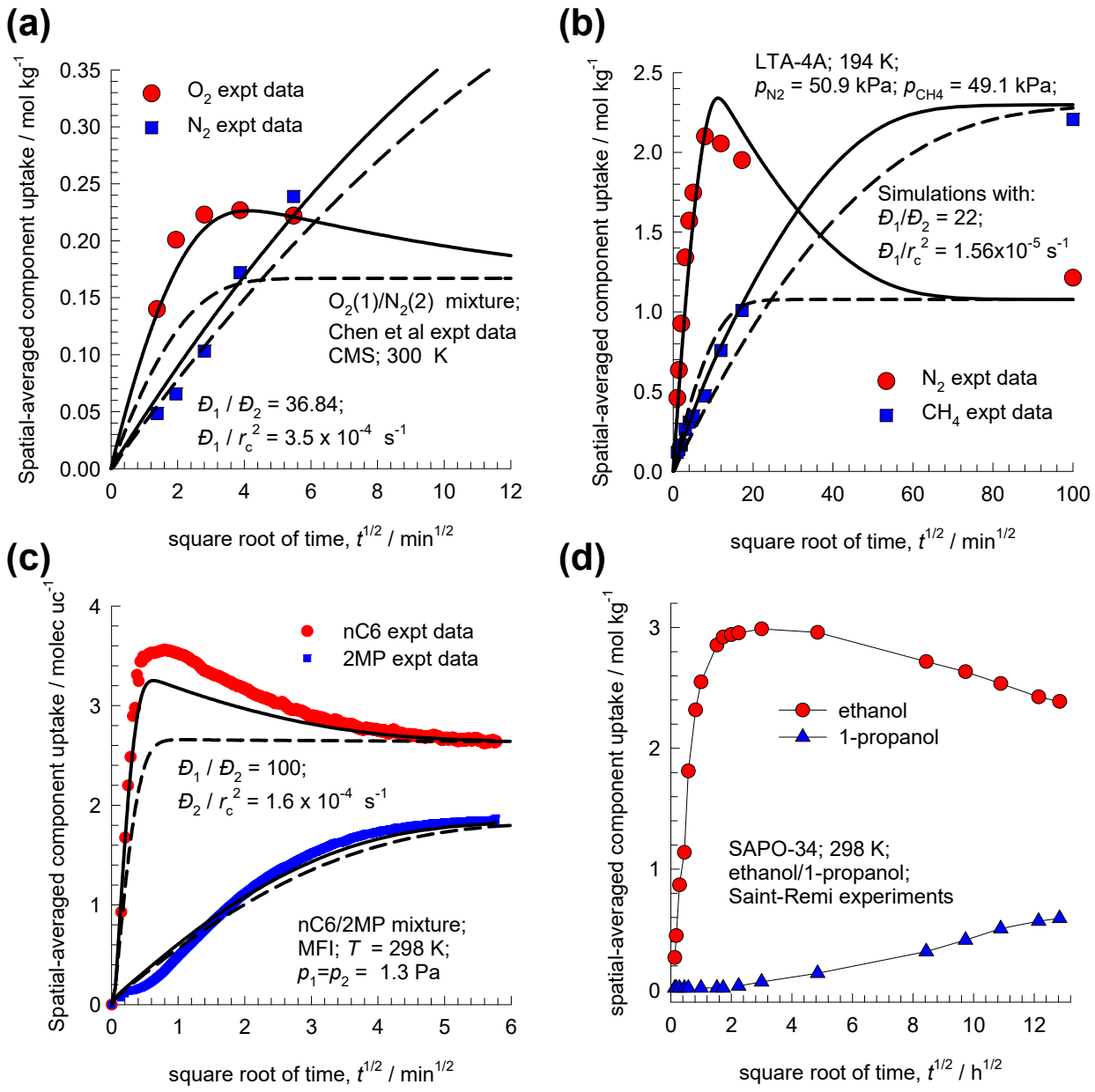

MS Fig 2

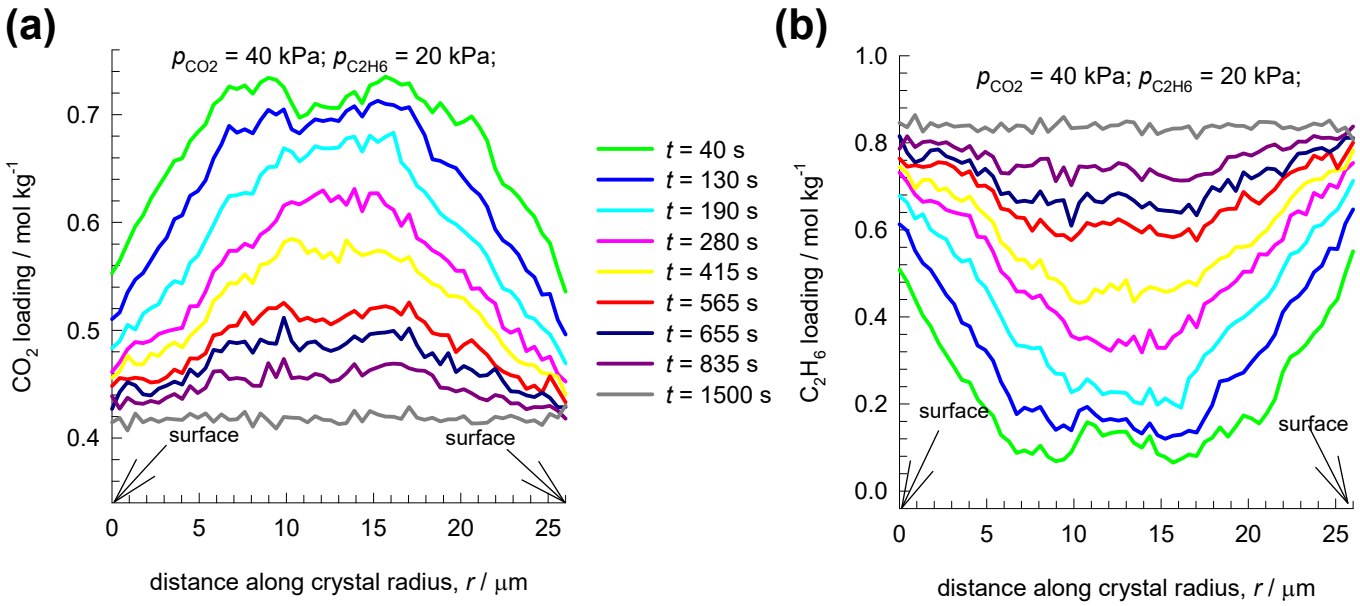

MS Fig 3

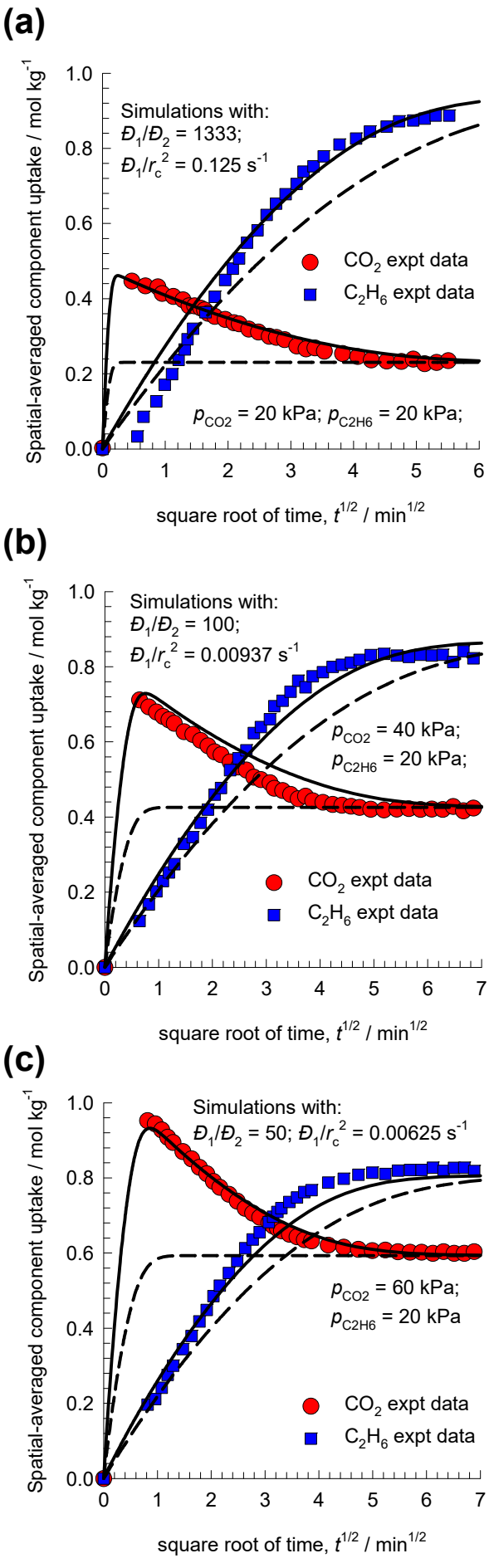

MS Fig 4

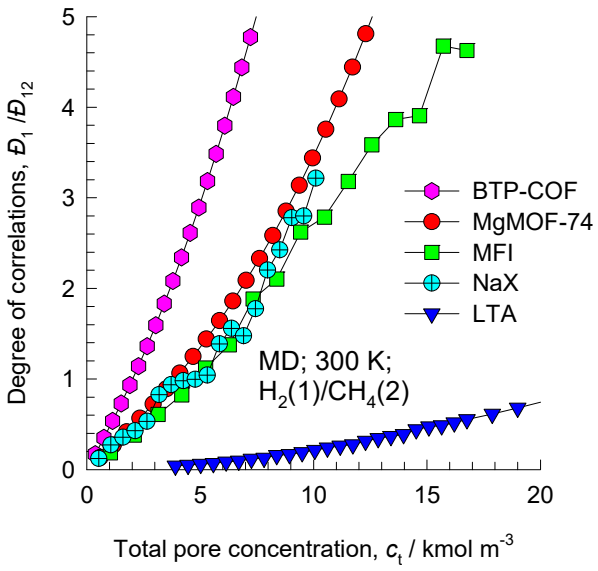

MS Fig 5

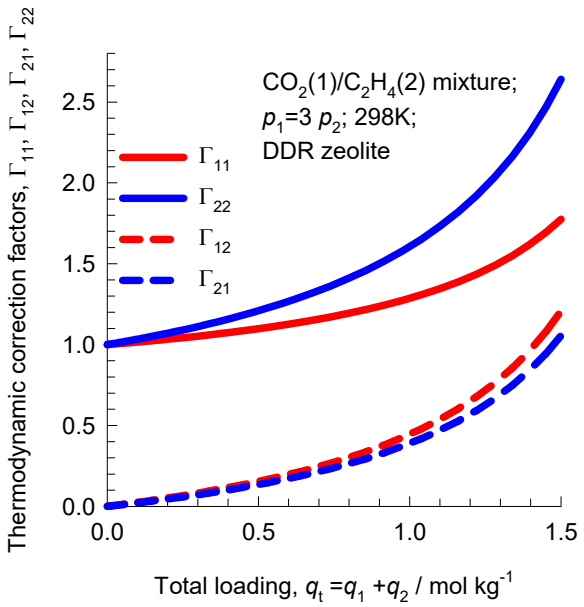

MS Fig 6

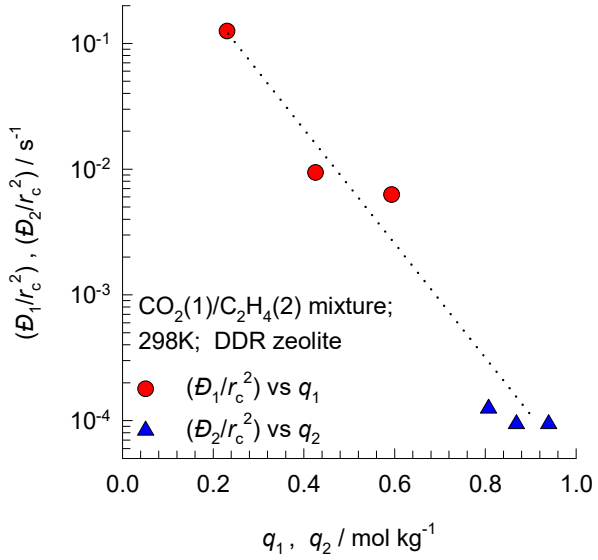

MS Fig 7

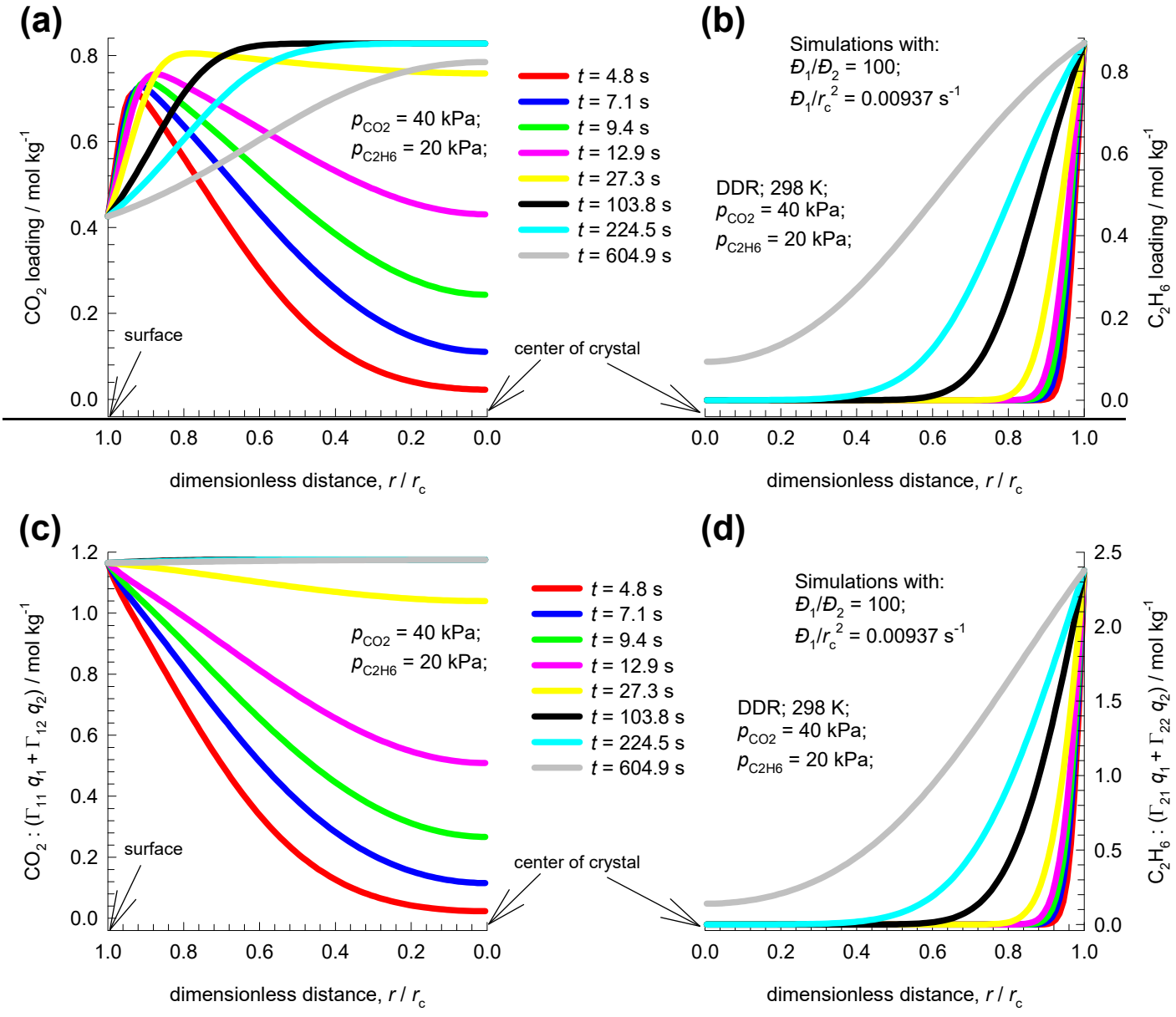

MS Fig 8

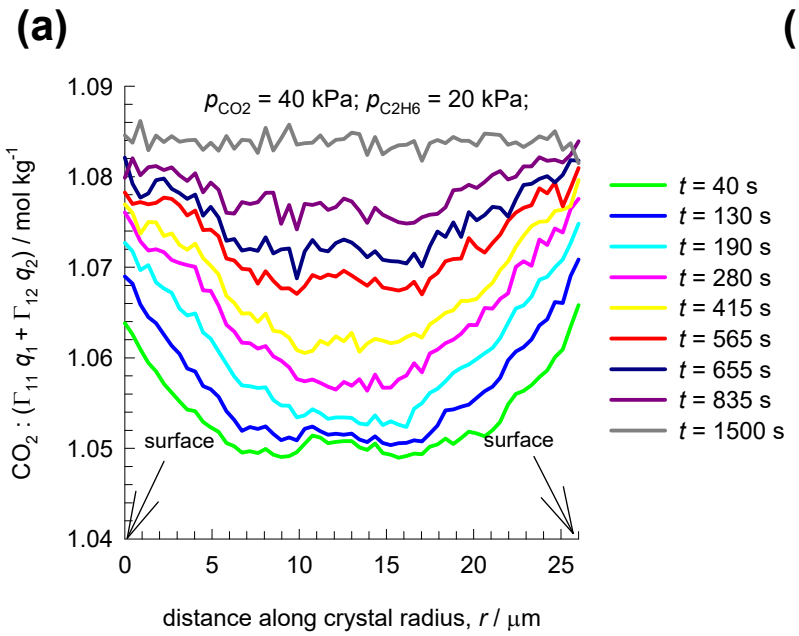

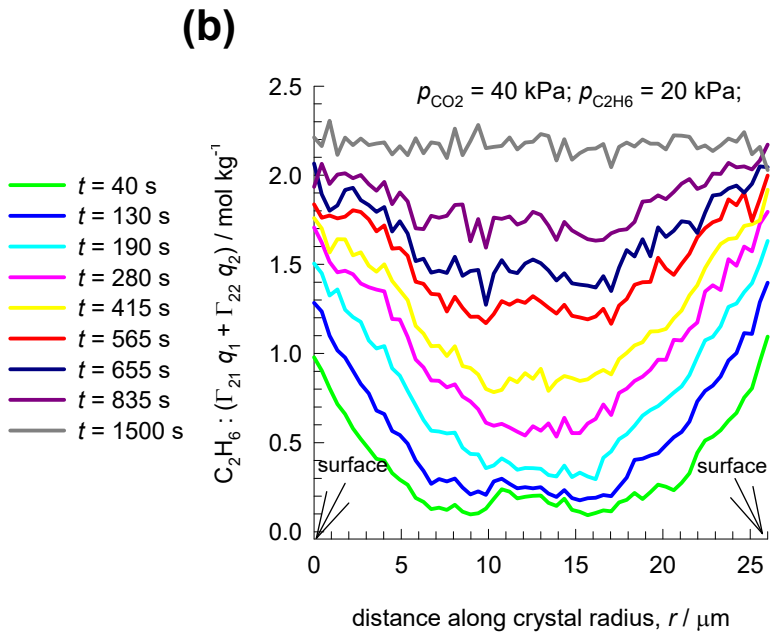

MS Fig 9

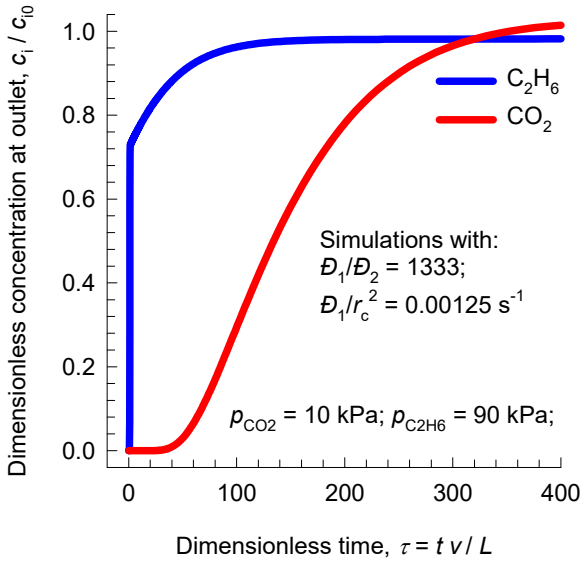

MS Fig 10

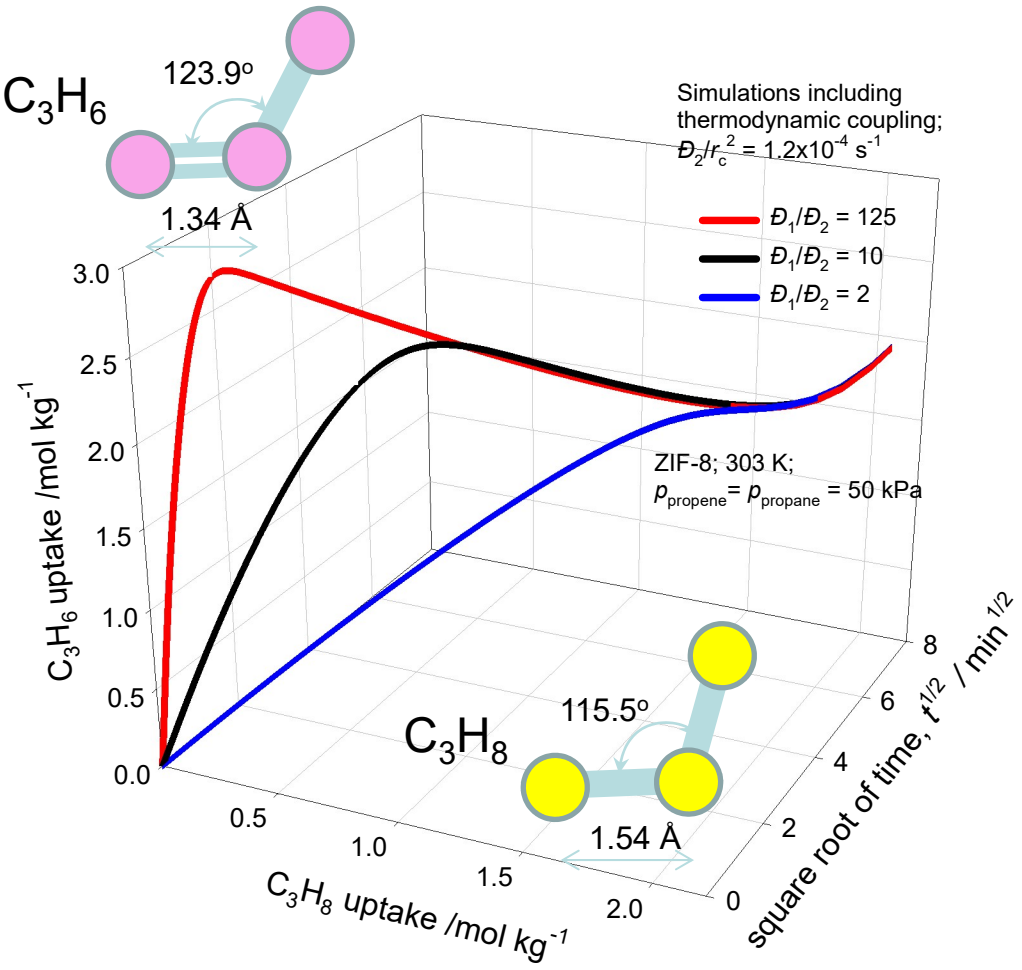

MS Fig 11

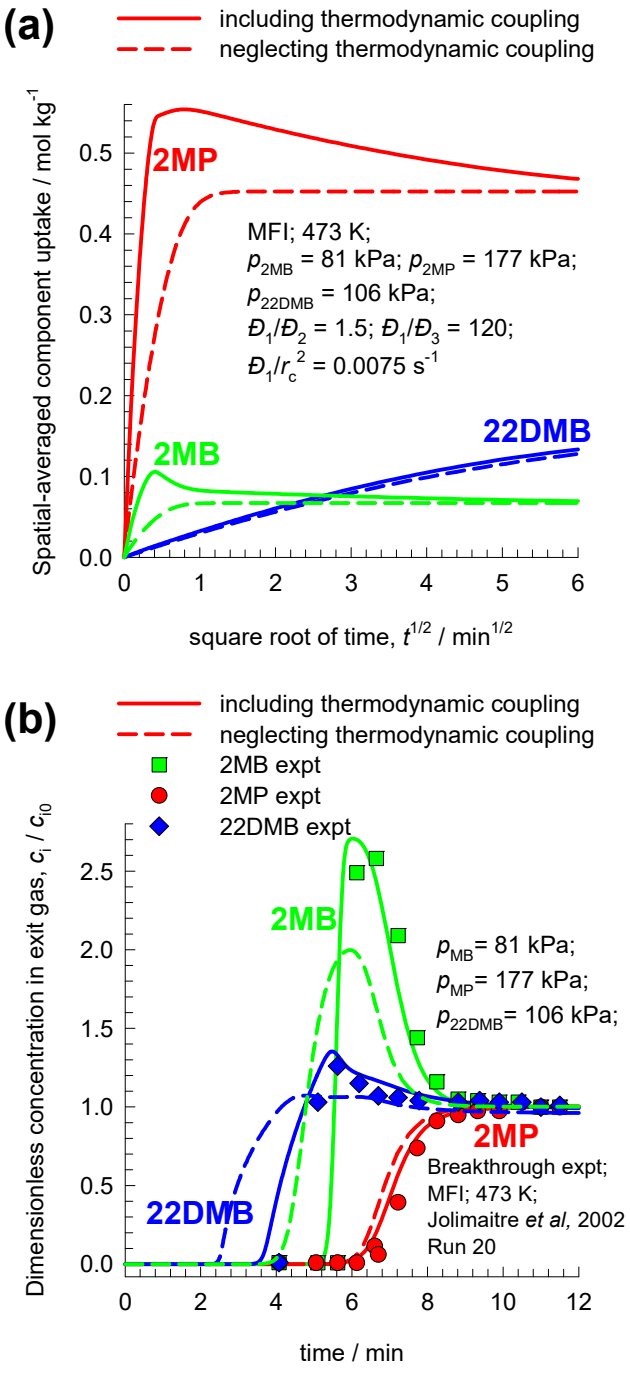

MS Fig 12

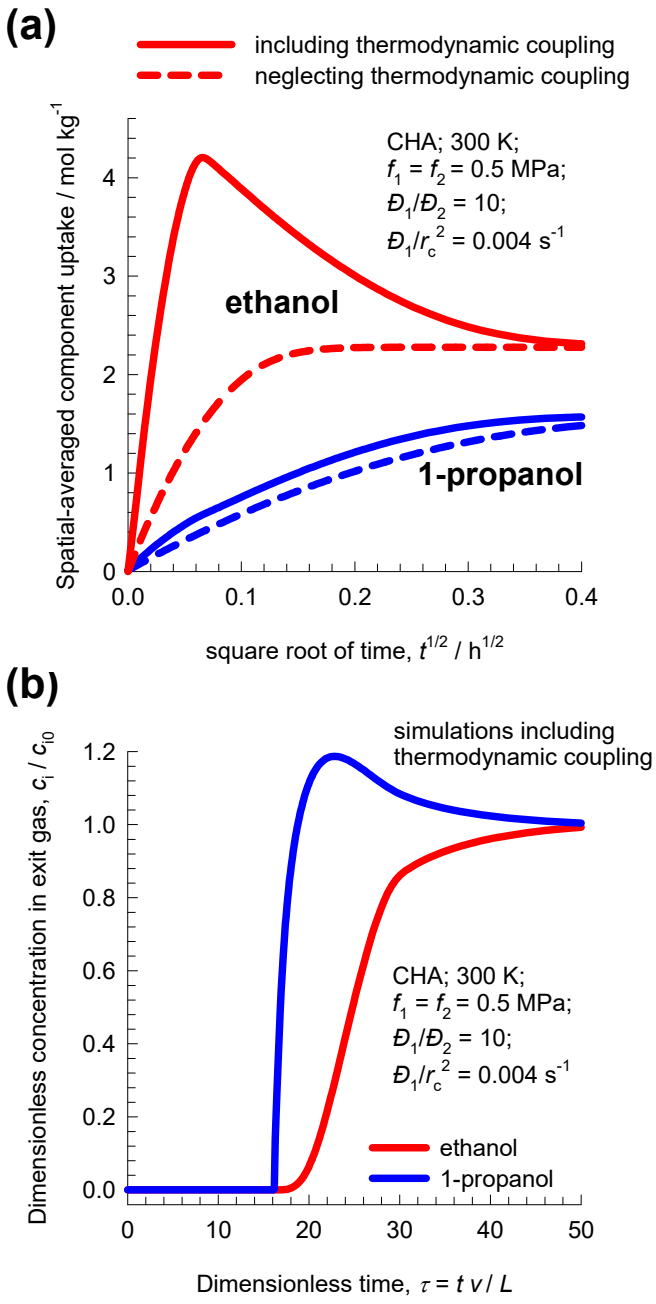

MS Fig 13

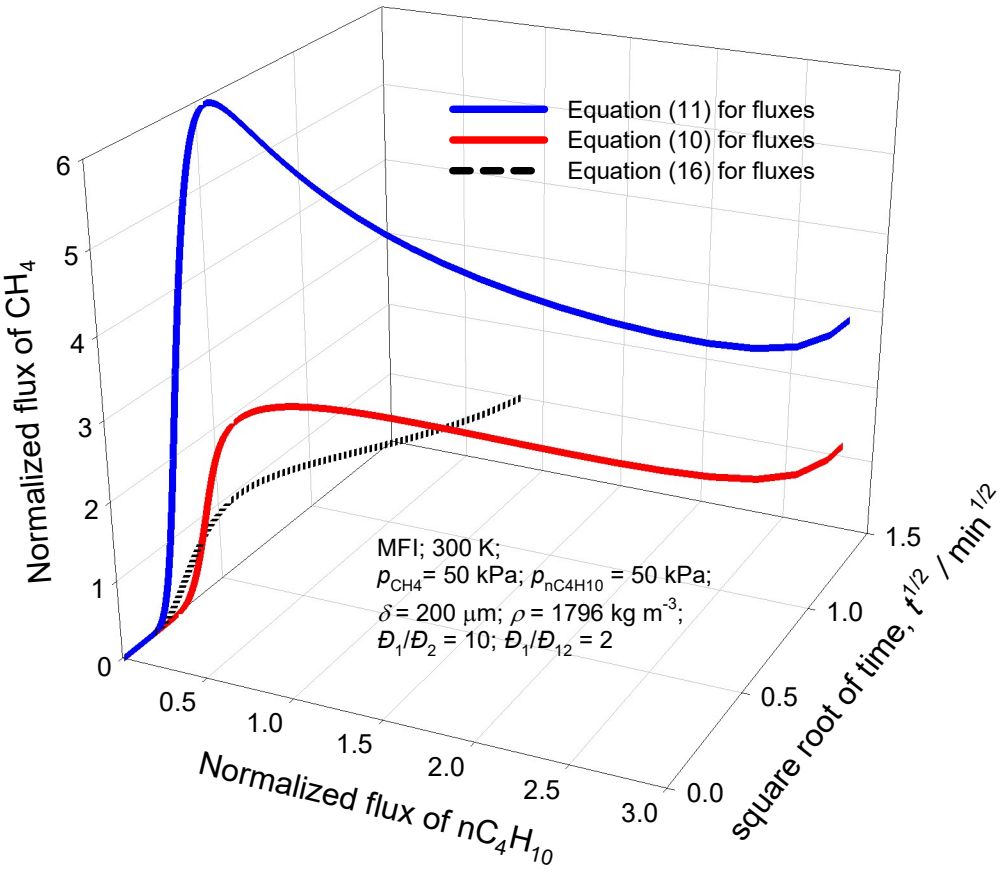

MS Fig 14